Solid Earth Discuss., https://doi.org/10.5194/se-2018-46
Manuscript under review for journal Solid Earth
Discussion started: 8 June 2018

Solid Earth Discussions
Open Access
EGU

The effect of rock composition on muon tomography measurements

Alessandro Lechmann[1], David Mair[1], Akitaka Ariga[2], Tomoko Ariga[3], Antonio Ereditato[2], Ryuichi Nishiyama[2], Ciro Pistillo[2], Paola Scampoli[2,4], Fritz Schlunegger[1], Mykhailo Vladymyrov[2]

[1]Institute of Geological Sciences, University of Bern, Bern, CH-3012, Switzerland
[2]Albert Einstein Center for Fundamental Physics, Laboratory for High Energy Physics, University of Bern, Bern, CH-3012, Switzerland
[3]Faculty of Arts and Science, Kyushu University, Fukuoka, J-812-8582, Japan
[4]Dipartimento di Fisica "E.Pancini", Università di Napoli Federico II, Napoli, I-80126, Italy

Correspondence to: Alessandro Lechmann (alessandro.lechmann@geo.unibe.ch)

Abstract. In recent years, the use of radiographic inspection with cosmic-ray muons has spread into multiple research and industrial fields. This technique is based on the high-penetration power of cosmogenic muons. Specifically, it allows the resolution of internal density structures of large scale, geological objects through precise measurement of the muon absorption rate. So far in many previous works, this muon absorption rate has been considered to depend solely on the density of traversed material (under the assumption of a standard rock) but the variation in chemical composition has not been taken seriously into account. However, from our experience with muon tomography in Alpine environments we find that this assumption causes a substantial bias on the muon flux calculation, particularly where the target consists of high $\{Z^2/A\}$ (like basalts) or low $\{Z^2/A\}$ (e.g. dolomites) rocks and where the material thickness exceeds 300 metres. In this paper we derive an energy loss equation for different minerals and we additionally derive a related equation for mineral assemblages that can be used for any rock type on which mineralogical data is available. Thus, for muon tomography experiments in which high/low $\{Z^2/A\}$ rock thicknesses can be expected, it is advisable to plan an accompanying geological field campaign to determine a realistic rock model.

1 Introduction

The discovery of the muon (Neddermeyer and Anderson, 1937) entailed experiments to characterise its propagation through different materials. The fact that muons lose energy proportionally to the mass density of the traversed matter (see Olive et al., 2014) inspired the idea of using their attenuation to retrieve information on the traversed material. This was first done by George (1955) for the estimation of the overburden upon building of a tunnel, and then later by Alvarez (1970) to search for hidden chambers in the pyramids at Giza (Egypt). In a related study, Fujii et al. (2013) employed this technology to allocate the reactor of a nuclear power plant. Recently, Morishima et al. (2017) successfully accomplished Alvarez' quest in the Egyptian Pyramids.

Solid Earth Discuss., https://doi.org/10.5194/se-2018-46
Manuscript under review for journal Solid Earth
Discussion started: 8 June 2018

Besides these applications, which have mainly been designed for archaeological and civil engineering purposes, scientists have begun to deploy particle detectors to investigate and map geological structures. In recent years this has been done for various volcanoes in Japan (Nishiyama et al., 2014; Tanaka et al., 2005, 2014), in the Caribbean and in France (Ambrosino et al., 2015; Jourde et al., 2013, 2015; Lesparre et al., 2012; Marteau et al., 2015). Recently, Barnaföldi et al. (2012) used this technology to examine karstic caves in the Hungarian mountains. Our group is presently carrying out an experimental campaign in the Central Swiss Alps (Nishiyama et al., 2017) aiming at imaging the glacier-bedrock interface, where we are faced with a variety of lithologies ranging from granitic, over paragneisic to carbonatic rocks that have a thickness larger than 500m.

Inferences about subsurface structures from observed muon flux (i.e. the number of muons recorded normalised by the exposure time and the detector acceptance) necessitate a comparison of the measurement data with muon flux simulations for structures with various densities. Such a simulation consists of a cosmic-ray muon energy spectrum model and a subsequent transportation of these muons through matter. The former describes the abundance of cosmic-ray muons for different energies and zenith angles at the surface of the earth. This has been well documented in literature (see for example Lesparre et al., 2010). The differences between the models, hence the systematic model uncertainty, can be as large as 10% for vertical muons. On the other hand, the attenuation of the muon flux is assumed to depend only on the density of the traversed material. In this context, however, effect of its chemical composition has not been taken into account properly. Previous works employ a certain representative rock, so-called “standard rock”, for which the rate of muon energy loss has been tabulated (e.g. Groom et al., 2001).

The origin of this peculiar rock type can be traced back to Hayman et al. (1963), Miyake et al. (1964), Mandò and Ronchi (1952) and George (1952), who gave slightly different definitions of its physical parameters (mass density ρ, atomic weight A and atomic number Z). A comprehensive compilation thereof can be found in table 1 of Higashi et al. (1966). Various corrections to the energy loss equation were then added in the framework of following up studies, which particularly includes a density effect correction (see for example Sternheimer et al., 1984). Richard-Serre (1971) listed next to soil from the CERN (European Organization for Nuclear Research) premises near Geneva (Switzerland) and Molasse-type material (e.g. Matter et al., 1980) also a “rock” that equals the one from Hayman et al. (1963). These latter authors assigned additional energy loss parameters to this particular rock type, which were similar to those of pure quartz. Lohmann et al. (1985) then adjusted these parameters to energy loss variables for calcium carbonate (i.e. limestone) and gave the standard rock its present representative. Summed up, this fictitious material consists of a density of crystalline quartz (i.e. 2.65 g/cm^3), a Z and A of 11 and 22, respectively (which is almost sodium), and density effect parameters that have been measured on calcium carbonate.

However, when the material's Z and A differ greatly from standard rock parameters as for carbonates, basalts or peridotites, a substantial bias would be introduced to the calculation of the muon flux. Since such a situation can be encountered easily in geological conditions such as the European Alps where igneous intrusions, thrusted and folded sedimentary covers and recent Quaternary deposits can be found in a rather narrow space (e.g. Schmid et al., 1996). Currently, the authors are performing a muon tomography experiment in the Jungfrau region, in the Central Swiss Alps, with the main focus on resolving the shape of the boundary between glaciers and the underlying bedrock (Ariga et al., 2018; Nishiyama et al., 2017). In this context, it turned out that the analyses based on the standard rock assumption might cause an over- or an underestimation of the bedrock position in our experiment. Such an uncertainty arising from the chemical composition of the actual rock has to be reduced at least to the level of the statistical uncertainty inherent in the measurement as well as in the systematic uncertainty of the muon energy spectrum model.

In this study, we investigate how different rock types potentially influence the results of a muon tomographic experiment. We particularly compare the lithologic effect on simulated data with standard rock data to estimate a systematic error that is solely induced by a too simplistic assumption on the composition of the bedrock.

2 Methods

2.1 Rock types

In this study we chose 10 different rock types that cover the largest range of natural lithologies, spanning the entire range from igneous to sedimentary rocks. The simplest rocks have a massive fabric in the sense that they do not exhibit any planar or porphyric texture. Lithologies with these characteristics are igneous and limestones (not sandstones as they might have a planar fabric such as laminations and ripples). Exemplary thin sections of a granite and a limestone are shown in Fig. 1. Note that metamorphic rocks are not treated in the framework of this study for simplicity purposes and will be subject of a follow-up paper. Also, for simplicity purposes, we do not consider spatial variations in crystal sizes in our calculations (i.e. a porphyric fabric). We justify this approach because a related inhomogeneity is likely to be averaged out if one considers a several m-thick rock column. Furthermore, the rock is considered to consist only of crystalline components, i.e. glassy materials such as obsidian have to be treated separately. Porous media can be approximated by assigning one of the constituents as air or (in the case of a pore fluid) water. This is explicitly done for the case of arkoses (10% air) and sandstones (11% air).

We compare the energy loss of muons in these rocks and hence the resultant muon flux attenuation depending on depth with those of the standard rock. The analysed lithologies together with their relevant physical parameters are listed in Table 1. Among these parameters, $\{Z/A\}$ and $\{Z^2/A\}$, i.e. the ratio of the atomic number (or its square) to the mass number averaged over the entire rock, are most relevant to the energy loss of muons. The former is almost proportional to the ionisation energy loss that occurs predominantly at low energies, whereas the latter is mostly proportional to the radiation energy loss,

Solid Earth Discuss., https://doi.org/10.5194/se-2018-46
Manuscript under review for journal Solid Earth
Discussion started: 8 June 2018

that becomes dominant for muons faster than their critical energy at around 600 GeV. The volumetric mineral fractions of these ten rocks can be found in Appendix A.

2.2 Cosmic ray flux model

We perform our calculations with the muon energy spectrum model proposed by Reyna (2006), at sea level and for vertical incident muons. This model describes the kinetic energy distribution of the muons before they enter the rock. The calculation of the integrated muon flux after having crossed a certain amount of material is done in two steps. First, the minimum energy required for muons to penetrate that given thickness of rock is calculated considering the chemical composition effects (see Sect. 2.3). Afterwards, the energy spectrum model is integrated above the obtained minimum energy (which we call from here on "cut-off energy", E_{cut}) to infinity, i.e.

$$I_{calc} = \int_{E_{cut}}^{\infty} \frac{dI(E)}{dE}\, dE. \quad (1)$$

The integration is necessary as most detectors, which have been used for muon tomography, record only the integrated muon flux.

2.3 Muon propagation in rocks

As soon as muons penetrate a material, they start to interact with the material's electrons and nuclei and lose part of their kinetic energy. The occurring processes can be categorised into an ionisation process, i.e. a continuous interaction with the material's electrons, and radiative interactions with the material's nuclei (i.e. bremsstrahlung, electron-positron pair production and photonuclear processes) which are of a stochastic nature. All these processes are governed by the material density ρ and the atomic number Z and atomic weight A (see Groom et al., 2001 for details). Our general strategy for the calculation of the energy loss in a rock is its decomposition into energy losses for the corresponding minerals. The energy loss of muons travelling a unit length in a rock can then be described by a volumetrically averaged energy loss through its mineral constituents

$$\left\{\frac{dE_{rock}}{dx}\right\} = \sum_j \varphi_j \left\langle \frac{dE_{mineral,j}}{dx} \right\rangle, \quad (2)$$

where φ_j is the volumetric fraction of the j-th mineral within the rock. The derivation of Eq. (2) can be found in Appendix B. In order to exploit this abstraction efficiently we have to assume a homogeneous mineral distribution within the rock. This is a strong simplification, considering for example effects related to a local intrusion, tectonic processes like folding and thrusting, or spatial differences in sedimentation patterns. These concerns can be addressed through averaging over a large enough volume. Figure 1 shows two typical thin-sections from rock samples of our experimental site that exhibit crystal sizes well below 1mm. As muon tomography for geological purposes generally operates at scales of 10-1000 m it is safe to

Solid Earth Discuss., https://doi.org/10.5194/se-2018-46
Manuscript under review for journal Solid Earth
Discussion started: 8 June 2018

assume that small-scale variations are averaged out. The term on the right-hand side of Eq. (2), i.e. the energy loss across each mineral, can be written as:

$$-\left\langle\frac{dE_{mineral}}{dx}\right\rangle = \rho_{\text{mineral}} * (\langle a\rangle + E * \langle b\rangle)\,, \tag{3}$$

where $\langle a\rangle$ and $\langle b\rangle$ are the ionisation and radiative energy losses across a given mineral, respectively. These two parameters are in turn calculated by averaging the contribution of each element (i.e. atom) constituting the mineral (see Eq. (B5) to Eq. (B15) in Appendix B for details). The density of the minerals, ρ_{mineral}, is estimated from its crystal structures (see Appendix A for more detailed instructions). Once the energy losses are obtained for all minerals, each contribution is summed up according to Eq. (2). The energy loss within the rock can then be expressed in a similar way, as in Eq. (3), (for a detailed discussion we refer to Appendix B):

$$-\left\{\frac{dE_{rock}}{dx}\right\} = \rho_{\text{rock}} * (\{a\} + E * \{b\})\,. \tag{4}$$

Again, the values $\{a\}$ and $\{b\}$ indicate the averaged ionisation and radiative energy losses across the whole rock, respectively. Eq. (4), an ordinary nonlinear differential equation, is usually given as a final value problem, i.e. we know that the muon, after having passed through the rock column, still needs some energy to penetrate the detector, E_{det}.This can be turned into an initial value problem, by reversing the sign Eq. (4) and defining the detector energy threshold as initial condition.

$$\left\{\frac{dE_{rock}}{dx}\right\} = \rho_{\text{rock}} * (\{a\} + E * \{b\}) \tag{5}$$

$$E(x = 0) = E_{det}$$

The problem has been transformed into the one of finding the final energy, the cut-off energy, E_{cut}, after a predefined thickness of rock. This is a well investigated problem, for which a great variety of numerical solvers are available. In this work we employ a standard Runge-Kutta integration scheme (see for example Stoer and Bulirsh, 2002).

3 Results

Figure 2 shows the muon flux simulations as a function of rock thicknesses up to 1 km for igneous and sedimentary rocks, respectively. The depth-intensity relation is described by a power law, as it is the integration of the differential energy spectrum of muons, which also follows a power law.

To better visualise the difference between the fluxes after having passed these ten rock types and the standard rock, we report in Fig. 3 the ratio between fluxes calculated after the different materials and that after the standard rock:

$$fr_{\text{rock}} = \frac{I_{calc,rock}}{I_{calc,SR}}\,. \tag{6}$$

Solid Earth Discuss., https://doi.org/10.5194/se-2018-46
Manuscript under review for journal Solid Earth
Discussion started: 8 June 2018

From Figs. 2 and 3 we can see that the attenuation of the muon flux depends predominantly on the rock density as expected. Rocks exhibiting a high material density result in a larger muon flux attenuation than lithologies with a lower density. This however, only depicts the overall differences, including density and compositional variations, between real and standard rock. In this regard, Groom et al. (2001) apply an explicit treatment of density variations of known materials. Thus, the flux data can be simulated for a standard rock with the exact density as its real counterpart. Such a density normalisation enables us to isolate the compositional influence on the computed data. Figure 4 represents the ratio between muon fluxes after passing through real rocks and the muon flux after passing through a density normalised standard rock. It is important to note that the standard rock muon flux in each flux ratio has been normalised with respect to the density of the original rock (i.e. the peridotite is compared to a standard rock of density ρ=3.340 g/cm^3, the limestone is comparted to a standard rock of density ρ=2.711 g/cm^3, etc.). One notices that the flux ratios are rather close together, mainly within 2.5% of the standard rock flux, before they start to diverge towards larger (dolomite, shale and arenite) and smaller (igneous rocks, arkose, limestone and aragonite) flux ratios beyond 300 m thickness of penetrated rock.

4 Discussion

The differences in the calculated muon flux illustrated in Fig. 2 become even more pronounced in Fig. 3, where the fluxes are compared to the case where cosmic fluxes are attenuated by a standard rock. One notices a direct correlation with material density. This statement is reinforced by the fact that the granite (Fig. 2) has almost the same density as the standard rock, 2.654 g/cm^3 vs. 2.650 g/cm^3, and shows an overall similar flux magnitude as the standard rock, i.e. a flux ratio of 1. This can be explained by Eq. (4), as the energy loss is almost directly proportional to the density, while the presence of density in the ionisation loss term (i.e. $\{a(E,\rho,A,Z)\}$) is negligible compared to this factor. Thus, if the rock flux data is compared to a standard rock with equal density this effect should be removed, and one is left with the bare composition difference.

A closer look to Fig. 4 reveals that the muon fluxes for every rock below 300 m do not depart more than 2.5% from their respective density modified standard rock flux. The chemical composition effect can thus be considered negligible when compared to the systematic uncertainty originating from the muon flux model. This is because of the dominance of the ionisation energy loss in this thickness region. Muons that penetrate down to 300 m of rock are still slow enough to predominantly lose their kinetic energy for ionisation of the rock's electrons. As the number of electrons per unit volume is given by the product: $\rho_{rock} * \{Z/A\}$, ionisation losses are proportional to this term. When comparing a density normalised standard rock with a real rock, the only difference can emerge from the second part, i.e. $\{Z/A\}$. According to Table 1 these values do not change more than 1% with respect to each other.

When the rock thicknesses become larger than 300 m, the flux ratios start to exceed +/- 2.5% and the ratio patterns diverge. This corresponds to the point where radiative losses start to become the dominant energy loss processes. The latter are interactions of the muon with the nuclei of the atoms within the rock and its cross section is mainly proportional to the square of the nucleus' charge (i.e. $\{Z^2/A\}$). Hence, rocks that exhibit a lower $\{Z^2/A\}$-value than standard rock (i.e. dolomite, arenite and shale) attenuate the muon flux less (i.e. flux ratio > 1), while all igneous rocks as well as limestone, aragonite and arkose, that have a higher $\{Z^2/A\}$-value attenuate the muon flux more, which results in a lower flux ratio.

The above results reflect only the most striking connections to the chemical composition of a rock. In reality however, the nature of muonic energy loss processes is much more complex as the shape of the flux ratios in Fig. 4 below 300 m suggests. The actual ionisation energy loss, Eq. (B27), is an interplay of the mean excitation energy $\{I\}$, i.e. the mean energy needed to ionise a material's electrons, material density ρ_{rock} , $\{Z/A\}$ and various correction terms that depend on these parameters. These additional factors are also responsible for the non-linear behaviour of the flux ratios between 100 m and around 600 m, as effects from radiative losses start to become significant. However, as resulting differences due to these processes remain smaller than 2.5%, a detailed discussion of these matters falls beyond the scope of this paper.

As we see above, the muon flux calculation is significantly biased when one employs the standard rock assumption and thus neglects the effect of the chemical composition, especially when the thickness of the rock is beyond 300 m. This systematic error would then later turn into an over- or an underestimation in the assesment of density structures. In particular, in case where the target is 600 m thick and made of dolomite ($\rho = 2.86\, g/cm^3$) for example, the standard rock assumption underestimates the flux by 7.5% and thus overestimates the density by $0.07\, g/cm^3$ or 2.5%. In cases where the determination of the thickness of the rock column is relevant, the effect would cause an underestimation of around 14 m, or 2.5%.

5 Conclusions

Our explorations suggest that it is safe to use the standard rock approximation for all rock types up to thicknesses of ~300 m, as the flux ratio will mainly remain within 2.5% of the standard rock flux, which generally lies within the cosmic ray flux model error. However, we also find that beyond these thicknesses the use of the standard rock approximation and its density-modified version could lead to a serious bias. This mainly concerns basaltic and carbonate rocks. Their error keeps increasing with growing material thickness up to a point where any inference based upon this approximation becomes difficult. It can be extrapolated, that these errors grow even further beyond 600m of material thickness. This is, however, a thickness range where muon tomography becomes increasingly hard to perform as lower fluxes have to be counterbalanced by larger detectors and longer exposure times.

Solid Earth Discuss., https://doi.org/10.5194/se-2018-46
Manuscript under review for journal Solid Earth
Discussion started: 8 June 2018

In order to account for the composition of rock it is advisable to undertake a geological study of the region alongside the muon tomography measurements, especially when faced with basaltic rocks or carbonates, which includes at the least the analysis of local rock samples. Auxiliary data could comprise pycnometer rock density measurements (i.e. He-pycnometer or buoyancy experiments), chemical composition, and mineralogical information (i.e. X-Ray diffractometry/fluorescence measurements) as well as microfabric analyses (i.e. mineral and fabric identification on thin sections). This additional information may help to constrain solutions of a subsequent inversion to a potentially smaller set. The use of additional information, such as spatial information in the form of a geological map or a 3D model of the geologic architecture, is strongly encouraged, because it might greatly improve the state of knowledge about the physical parameters that are to be unravelled.

Solid Earth Discuss., https://doi.org/10.5194/se-2018-46
Manuscript under review for journal Solid Earth
Discussion started: 8 June 2018

Appendix A

To estimate the mineral density, we assume that it can be calculated by dividing the mass of the atoms within the crystal unit cell by the volume of the latter (see for example Borchart-Ott, 2009):

$$\rho_{mineral} = \frac{Q*M}{N_A*V_{Unit\ Cell}}\,. \tag{A1}$$

In this equation, M is the total molar mass of one mineral "formula unit", Q is the number of formula units per unit cell and $V_{Unit\ Cell}$ is the volume of the unit cell. The latter is calculated by the volume formula of a parallelepiped:

$$V_{Unit\ Cell} = \left\|\vec{a}\cdot\left(\vec{b}\times\vec{c}\right)\right\|. \tag{A2}$$

Eq. (A2) can be rewritten as

$$V_{Unit\ Cell} = \|\vec{a}\|\left\|\vec{b}\right\|\|\vec{c}\|\sqrt{1+2\cos(\alpha)\cos(\beta)\cos(\gamma)-\cos^2(\alpha)-\cos^2(\beta)-\cos^2(\gamma)}\,. \tag{A3}$$

Here, $\vec{a},\vec{b},\vec{c}$ denote the unit cell vectors, their lengths, $\|\cdot\|$, measured in Ångströms, whereas α,β,γ are the internal angles between those vectors. These six parameters can be looked up for each mineral in the crystallographic literature (e.g. Strunz and Nickel, 2001).

The volumetric percentages of the minerals that constitute the 10 investigated rock types are shown in Table A1 and Table A2. They were chosen as a reasonable compromise from literature values (e.g. Best, 2003; Tuttle and Bowen, 1958; Folk, 1980).

Solid Earth Discuss., https://doi.org/10.5194/se-2018-46
Manuscript under review for journal Solid Earth
Discussion started: 8 June 2018

Appendix B

Energy loss in elements

The average spatial differential energy loss can be written in a rather simple form (Barrett et al., 1952):

$$-\left(\frac{dE(\rho,A,Z)}{dx}\right) = \rho * (a(E,\rho,A,Z) + E * b(E,A,Z)). \quad \text{(B1)}$$

Here, ρ, A, Z denote the mass density, atomic weight and atomic number of the penetrated material, while E is the kinetic energy of the penetrating, charged particle and x is the position coordinate. The function $a(E,\rho,A,Z)$ in Eq. (B1) is the differential ionisation energy loss that accounts for the ionisation of electrons of the penetrated material. In the case of incident muons (i.e. electric charge $q_\mu = -1\,C$ and mass $m_\mu = 105.7\,MeV/c^2$), the relationships expressed in Eq. (B1) takes the form (see e.g. Olive et al., 2014 for a detailed explanation):

$$a(E,\rho,A,Z) = K\frac{Z}{A}\frac{1}{\beta^2}\left[\frac{1}{2}\,ln\left(\frac{2m_e c^2\beta^2\gamma^2 Q_{max}(\mathrm{E})}{I(Z)^2}\right) - \beta^2 - \frac{\delta(\rho,Z,A)}{2} + \frac{1}{8}\frac{Q^2_{max}(\mathrm{E})}{\left(\gamma \mathrm{m}_\mu c^2\right)^2}\right] + \Delta\left|\frac{dE}{dX}\right|(Z,A)\,. \quad \text{(B2)}$$

In this equation, β, γ are the relativistic factors and are, therefore, a function of the kinetic energy E. In contrast, the function $b(E,A,Z)$ describes all the radiative processes that become dominant at higher velocities (above ~600 GeV/c for muons). This term includes energy losses due to bremsstrahlung, electron-positron pair production as well as photonuclear interactions. These different contributions can be written independently from each other:

$$b(E,A,Z) = b_{brems}(E,A,Z) + b_{pair}(E,A,Z) + \mathrm{b}_{photonucl}(E,A,Z). \quad \text{(B3)}$$

Each process in Eq. (B3) is computed by integrating its differential cross-section with respect to every possible amount of transferred energy:

$$b_{process} = \frac{N_A}{A}\int_0^1 \nu\,\frac{d\sigma_{process}}{d\nu}\,d\nu. \quad \text{(B4)}$$

Here, N_A is the Avogadro number and $\nu = \varepsilon/E$ the fractional energy loss (whereas ε is the absolute energy loss) for this process. The differential cross-sections for bremsstrahlung (Kelner et al., 1995, 1997) and photonuclear (Bezrukov and Bugaev, 1981) energy losses are used by Groom et al. (2001) for the calculations of their tables, whereas the pair-production cross-section (Kelner, 1998; Kokoulin and Petrukhin, 1969, 1971) is used in GEANT4 (Agostinelli et al., 2003) by default. The latter has been taken from the GEANT4 simulation toolkit for computational purposes, as the pair-production cross-section (Nikishov, 1978) applied in the study of Groom et al. (2001) involves the calculation of many computationally extensive dilogarithms.

Solid Earth Discuss., https://doi.org/10.5194/se-2018-46
Manuscript under review for journal Solid Earth
Discussion started: 8 June 2018

Energy loss in minerals

Since the above equations are valid for pure elements, their adjustments are needed for compounds (e.g. minerals) and mixtures thereof (e.g. rocks). Generally, it is advised to use the physical parameters for materials that have already been measured (see Seltzer and Berger, 1982 for a compilation). However, except for calcium carbonate (i.e., calcite) and silicon dioxide (i.e. quartz), no other minerals have been investigated. This also means that there is no standard approach available for considering natural rocks. Fortunately, for such materials a theoretical framework has been proposed (see for example Appendix A of Groom et al., 2001). The basic idea is to consider the compound as a single "weighted average"-material and the energy loss therein as a mass weighted average of its constituents' energy loss:

$$\left\langle \frac{dE_{mineral}}{d\chi} \right\rangle = \sum_i w_i \left(\frac{dE_{element,i}}{d\chi} \right). \tag{B5}$$

The weights w_i are calculated according to the atomic weights A_i of the elements:

$$w_i = \frac{n_i A_i}{\sum_k n_k A_k} = \frac{m_{element,i}}{m_{mineral}}. \tag{B6}$$

These weights w_i can now be used to calculate an average $\langle Z/A \rangle$ value:

$$\left\langle \frac{Z}{A} \right\rangle = \sum_i w_i \frac{Z_i}{A_i}. \tag{B7}$$

Equivalently, the average $\langle Z^2/A \rangle$ value can be calculated according to

$$\left\langle \frac{Z^2}{A} \right\rangle = \sum_i w_i \frac{Z_i^2}{A_i}. \tag{B8}$$

One more change must be made to the ionisation loss Eq. (B2) in order to appropriately account for the change in the atomic structure that emerged due to chemical bonding of the elementary constituents. This is reflected in a modified mean excitation energy $\langle I \rangle$, which can be calculated by taking the exponential of the function

$$\ln\langle I \rangle = \frac{\sum_i w_i \frac{Z_i}{A_i} \ln(I_i)}{\sum_j w_j \frac{Z_j}{A_j}}, \tag{B9}$$

which is basically a weighted geometric average of the elementary mean excitation energies

$$\langle I \rangle = \sqrt[\sum_j w_j \frac{Z_j}{A_j}]{\prod_i I_i^{w_i \frac{Z_i}{A_i}}}. \tag{B10}$$

Solid Earth Discuss., https://doi.org/10.5194/se-2018-46
Manuscript under review for journal Solid Earth
Discussion started: 8 June 2018

One has to pay attention that the mean excitation energies for some elements, I_i, can change quite significantly when they are part of a chemical bond. A guideline to address this issue can be found in Seltzer and Berger (Seltzer and Berger, 1982). Equations (B7) to (B10) are still a consequence of Eq. (B5). However, there is one term in the function $\delta(\rho, Z/A)$ in Eq. (B2) that is calculated differently from Eq. (B5). Namely the logarithm of the plasma energy of the compound, which for an element is given by (e.g. Olive et al., 2014):

$$\ln(\hbar\omega_p) = \ln\left(28.816 * \sqrt{\rho\frac{Z}{A}}\right). \quad \text{(B11)}$$

According to Eq. (B5) the plasma energy for a compound should be calculated the same way as the mean excitation energy in Eq. (B9). However, Sternheimer et al. (1982) and Fano (1963) explicitly tell us to use the arithmetic mean within the logarithm when dealing with an atomic mixture (i.e. a molecule), yielding

$$\ln\langle\hbar\omega_p\rangle = \ln\left(28.816 * \sqrt{\rho_{mineral}\langle\frac{Z}{A}\rangle}\right). \quad \text{(B12)}$$

This results in the modified ionisation energy loss:

$$\langle a(E, \rho_{mineral}, A, Z)\rangle = K\langle\frac{Z}{A}\rangle\frac{1}{\beta^2}\left[\frac{1}{2}\,ln\left(\frac{2m_e c^2\beta^2\gamma^2 Q_{max}(\mathrm{E})}{\langle I(Z)\rangle^2}\right) - \beta^2 - \frac{\delta\left(\rho_{mineral},\langle\frac{Z}{A}\rangle\right)}{2} + \frac{1}{8}\frac{Q^2_{max}(\mathrm{E})}{(\gamma \mathrm{m}_\mu c^2)^2}\right] + \Delta\left|\frac{dE}{dX}\right|\left(\langle\frac{Z}{A}\rangle\right). \quad \text{(B13)}$$

The radiation loss for the compound, on the other hand, is only a linear combination of the radiation losses of its elementary constituents, Eq. (B3), yielding:

$$\langle b\rangle = \sum_i w_i b_i\,. \quad \text{(B14)}$$

The resulting Eq. (B15)

$$-\langle\frac{dE_{mineral}}{dx}\rangle = \rho_{\mathrm{mineral}} * (\langle a\rangle + E * \langle b\rangle)\,, \quad \text{(B15)}$$

has now the same form as the energy loss Eq. (B1) for elements and can be solved accordingly.

Energy loss in rocks

To obtain an energy loss equation for rocks, a similar procedure as for forming minerals out of elements can be applied. Starting from Eq. (B5) we consider the energy loss for a rock as mass weighted average of the energy losses of its mineral constituents

Solid Earth Discuss., https://doi.org/10.5194/se-2018-46
Manuscript under review for journal Solid Earth
Discussion started: 8 June 2018

$$\left\langle \frac{dE_{rock}}{d\chi} \right\rangle = \sum_j q_j \left\langle \frac{dE_{mineral,j}}{d\chi} \right\rangle , \quad \text{(B16)}$$

where q_j are the mass fractions of the j-th mineral within the rock, analogous to Eq. (B6),

$$\mathrm{q_j} = \frac{n_j A_j}{\sum_l n_l A_l} = \frac{m_{mineral,j}}{m_{rock}} . \quad \text{(B17)}$$

Using $d\chi = \rho * dx$, Eq. (B16) then takes the following form:

$$\frac{1}{\rho_{rock}} \left\langle \frac{dE_{rock}}{dx} \right\rangle = \sum_j \frac{\mathrm{q_j}}{\mathrm{\rho_{mineral,j}}} \left\langle \frac{dE_{mineral,j}}{dx} \right\rangle . \quad \text{(B18)}$$

By inserting Eq. (B17) into Eq. (B18), one obtains

$$\frac{1}{\rho_{rock}} \left\langle \frac{dE_{rock}}{dx} \right\rangle = \frac{1}{\mathrm{m_{rock}}} \sum_j \frac{\mathrm{m_{mineral,j}}}{\mathrm{\rho_{mineral,j}}} \left\langle \frac{dE_{mineral,j}}{dx} \right\rangle . \quad \text{(B19)}$$

Multiplying both sides with ρ_{rock} and applying the definition of the density, $\rho = m/v$, that can also be written as $v = m/\rho$, Eq. (B19) becomes

$$\left\langle \frac{dE_{rock}}{dx} \right\rangle = \frac{1}{\mathrm{v_{rock}}} \sum_j \mathrm{v_{mineral,j}} \left\langle \frac{dE_{mineral,j}}{dx} \right\rangle . \quad \text{(B20)}$$

If one sets $\varphi_j = v_{mineral,j}/v_{rock}$, the volumetric fraction of the j-th mineral within the rock, Eq. (B20) transforms into the compound equation for rocks

$$\left\langle \frac{dE_{rock}}{dx} \right\rangle = \sum_j \varphi_j \left\langle \frac{dE_{mineral,j}}{dx} \right\rangle . \quad \text{(B21)}$$

Analogue to the mineral case we can now define new average energy loss parameters for the rock, beginning with its overall density

$$\{\rho_{rock}\} = \sum_j \varphi_j \, \rho_{mineral,j} . \quad \text{(B22)}$$

The average $\{Z/A\}$ is given by

$$\left\{\frac{Z}{A}\right\} = \sum_j \frac{\rho_{mineral,j}}{\rho_{rock}} \varphi_j \left\langle \frac{Z}{A} \right\rangle_j \quad \text{(B23)}$$

and similarly, the average $\{Z^2/A\}$ can be calculated according to

$$\left\{\frac{Z^2}{A}\right\} = \sum_j \frac{\rho_{mineral,j}}{\rho_{rock}} \varphi_j \left\langle \frac{Z^2}{A} \right\rangle_j . \quad \text{(B24)}$$

Solid Earth Discuss., https://doi.org/10.5194/se-2018-46
Manuscript under review for journal Solid Earth
Discussion started: 8 June 2018

The rock's mean excitation energy is

$$\ln\{I\} = \frac{\sum_j \frac{\rho_{mineral,j}}{\rho_{rock}} \varphi_j \langle \frac{Z}{A} \rangle_j \ln\langle I \rangle_j}{\sum_l \frac{\rho_{mineral,l}}{\rho_{rock}} \varphi_l \langle \frac{Z}{A} \rangle_l} . \quad \text{(B25)}$$

The only difference between the rock calculation and the mineral calculation enters in the calculation of the plasma energy. While in the mineral case we were advised to use Eq. (B11) instead of what would naturally follow from the weighted average in Eq. (B5), we prefer to use the weighted average, Eq. (B21),

$$\ln\{\hbar\omega_p\} = \frac{\sum_j \frac{\rho_{mineral,j}}{\rho_{rock}} \varphi_j \langle \frac{Z}{A} \rangle_j \ln\langle \hbar\omega_p \rangle_j}{\sum_l \frac{\rho_{mineral,l}}{\rho_{rock}} \varphi_l \langle \frac{Z}{A} \rangle_l} \quad \text{(B26)}$$

for the case of rocks. The reason for this lies in the fact that the density effect operates on a nanometric scale, whereas minerals, in general have sizes between several micrometres and a few centimetres. In the case of a mineral compound, the molecular structure is also on a nanometric scale.

These parameters can then be rearranged into an ionisation loss term for a rock

$$\{a(E, \rho_{rock}, A, Z)\} = K \left\{\frac{Z}{A}\right\} \frac{1}{\beta^2} \left[\frac{1}{2} ln\left(\frac{2m_e c^2 \beta^2 \gamma^2 Q_{max}(\mathrm{E})}{\{I(Z)\}^2}\right) - \beta^2 - \frac{\delta\left(\rho_{rock}, \left\{\frac{Z}{A}\right\}\right)}{2} + \frac{1}{8} \frac{Q_{max}^2(\mathrm{E})}{\left(\gamma \mathrm{m}_\mu c^2\right)^2}\right] + \Delta \left|\frac{dE}{dX}\right| \left(\left\{\frac{Z}{A}\right\}\right) . \quad \text{(B27)}$$

Like Eq. (B14) the radiative losses can be rewritten as a weighted average of the mineral radiative losses

$$\{b\} = \sum_j \frac{\rho_{mineral,j}}{\rho_{rock}} \varphi_j \langle b \rangle_j . \quad \text{(B28)}$$

Equations. (B27) and (B28) can then be joined together to form again a similar term to Eqs. (B1) and (B15),

$$-\left\{\frac{dE_{rock}}{dx}\right\} = \rho_{\mathrm{rock}} * (\{a\} + E * \{b\}) , \quad \text{(B29)}$$

the energy loss equation for rocks.

Acknowledgements

We thank the Jungfrau Railway Company for their continuing logistic support during our fieldwork in the central Swiss alps. We want also to thank the High-Altitude Research Stations Jungfraujoch & Gornergrat for providing us with access to their research facilities and accommodation. Furthermore, we thank the Swiss National Science Foundation (project No 159299 awarded to F. Schlunegger and A. Ereditato) for their financial support of this research project.

Author contributions

AL, FS and AE designed the study
AL developed the code with contributions by MV
AL performed the numerical experiments with support by RN
Geological data was compiled by DM and AL
AA, TA, PS, RN and CP verified the outcome of the numerical experiments
AL wrote the text with contributions from all co-authors
AL designed the figures with contributions by DM
All co-authors contributed to the discussion and finally approved the manuscript

Agostinelli, S., Allison, J., Amako, K., Apostolakis, J., Araujo, H., Arce, P., Asai, M., Axen, D., Banerjee, S., Barrand, G., Behner, F., Bellagamba, L., Boudreau, J., Broglia, L., Brunengo, A., Burkhardt, H., Chauvie, S., Chuma, J., Chytracek, R., Cooperman, G., Cosmo, G., Degtyarenko, P., Dell'Acqua, A., Depaola, G., Dietrich, D., Enami, R., Feliciello, A., Ferguson, C., Fesefeldt, H., Folger, G., Foppiano, F., Forti, A., Garelli, S., Giani, S., Giannitrapani, R., Gibin, D., Gomez Cadenas, J. J., Gonzalez, I., Gracia Abril, G., Greeniaus, G., Greiner, W., Grichine, V., Grossheim, A., Guatelli, S., Gumplinger, P., Hamatsu, R., Hashimoto, K., Hasui, H., Heikkinen, A., Howard, A., Ivanchenko, V., Johnson, A., Jones, F. W., Kallenbach, J., Kanaya, N., Kawabata, M., Kawabata, Y., Kawaguti, M., Kelner, S., Kent, P., Kimura, A., Kodama, T., Kokoulin, R., Kossov, M., Kurashige, H., Lamanna, E., Lampen, T., Lara, V., Lefebure, V., Lei, F., Liendl, M., Lockman, W., Longo, F., Magni, S., Maire, M., Medernach, E., Minamimoto, K., Mora de Freitas, P., Morita, Y., Murakami, K., Nagamatu, M., Nartallo, R., Nieminen, P., Nishimura, T., Ohtsubo, K., Okamura, M., O'Neale, S., Oohata, Y., Paech, K., Perl, J., Pfeiffer, A., Pia, M. G., Ranjard, F., Rybin, A., Sadilov, S., di Salvo, E., Santin, G., Sasaki, T., Savvas, N., et al.: GEANT4 - A simulation toolkit, Nucl. Instruments Methods Phys. Res. Sect. A Accel. Spectrometers, Detect. Assoc. Equip., 506, 250–303, doi:10.1016/S0168-9002(03)01368-8, 2003.

Alvarez, L. W., Anderson, J. A., Bedwei, F. E., Burkhard, J., Fakhry, A., Girgis, A., Goneid, A., Hassan, F., Iverson, D., Lynch, G., Miligy, Z., Moussa, A. H., Sharkawi, M. and Yazolino, L.: Search for Hidden Chambers in the Pyramids, Science (80-.)., 167, 832–839, doi:10.1126/science.167.3919.832, 1970.

Ambrosino, F., Anastasio, A., Bross, A., Béné, S., Boivin, P., Bonechi, L., Cârloganu, C., Ciaranfi, R., Cimmino, L., Combaret, C., D'Alessandro, R., Durand, S., Fehr, F., Français, V., Garufi, F., Gailler, L., Labazuy, P., Laktineh, I., Lénat, J.-F., Masone, V., Miallier, D., Mirabito, L., Morel, L., Mori, N., Niess, V., Noli, P., Pla-Dalmau, A., Portal, A., Rubinov, P., Saracino, G., Scarlini, E., Strolin, P. and Vulpescu, B.: Joint measurement of the atmospheric muon flux through the Puy de Dôme volcano with plastic scintillators and Resistive Plate Chambers detectors, J. Geophys. Res. Solid Earth, 120, 1–18, doi:10.1002/2015JB011969, 2015.

Ariga, A., Ariga, T., Ereditato, A., Käser, S., Lechmann, A., Mair, D., Nishiyama, R., Pistillo, C., Scampoli, P., Schlunegger, F. and Vladymyrov, M.: A Nuclear Emulsion Detector for the Muon Radiography of a Glacier Structure, Instruments, 2, 1–13, doi:10.3390/instruments2020007, 2018.

Barnaföldi, G. G., Hamar, G., Melegh, H. G., Oláh, L., Surányi, G. and Varga, D.: Portable cosmic muon telescope for environmental applications, Nucl. Instruments Methods Phys. Res. Sect. A Accel. Spectrometers, Detect. Assoc. Equip., 689, 60–69, doi:10.1016/j.nima.2012.06.015, 2012.

Barrett, P. H., Bollinger, L. M., Cocconi, G., Eisenberg, Y. and Greisen, K.: Interpretation of cosmic-ray measurements far underground, Rev. Mod. Phys., 24, 133–178, doi:10.1103/RevModPhys.24.133, 1952.

Best, M. G.: Igneous and metamorphic petrology, 2nd ed., Blackwell Science Ltd., 2003.

Bezrukov, L. B. and Bugaev, E. V.: Nucleon shadowing effects in photonuclear interaction, Sov. J. Nucl. Phys., 33, 635–641, 1981.

Borchardt-Ott, W.: Kristallographie, Springer Berlin Heidelberg, Berlin, Heidelberg., 2009.

Fano, U.: Penetration of protons, alpha particles, and mesons, Annu. Rev. Nucl. Sci., 13, 1–66, 1963.

Folk, R. L.: Petrology of the sedimentary rocks, Hemphill Publishing Company., 1980.

Fujii, H., Hara, K., Hashimoto, S., Ito, F., Kakuno, H., Kim, S. H., Kochiyama, M., Nagamine, K., Suzuki, A., Takada, Y., Takahashi, Y., Takasaki, F. and Yamashita, S.: Performance of a remotely located muon radiography system to identify the inner structure of a nuclear plant, Prog. Theor. Exp. Phys., 2013, 73C01-0, doi:10.1093/ptep/ptt046, 2013.

George, E. P.: Observations of cosmic rays underground and their interpretation, in Process in Cosmic Ray Physics, vol. 1, pp. 395–451., 1952.

George, E. P.: Cosmic rays measure overburden of tunnel, Commonw. Eng., 455, 1955.

Groom, D. E., Mokhov, N. V. and Striganov, S. I.: MUON STOPPING POWER AND RANGE TABLES 10 MeV–100 TeV, At. Data Nucl. Data Tables, 78, 183–356, doi:10.1006/adnd.2001.0861, 2001.

Hayman, P. J., Palmer, N. S. and Wolfendale, A. W.: The Rate of Energy Loss of High-Energy Cosmic Ray Muons, Proc. R. Soc. A Math. Phys. Eng. Sci., 275, 391–410, doi:10.1098/rspa.1963.0176, 1963.

Higashi, S., Kitamura, T., Miyamoto, S., Mishima, Y., Takahashi, T. and Watase, Y.: Cosmic-Ray Intensities under Sea-Water at Depths Down to 1400 m, Nuovo Cim., 10, 334–346, 1966.

Jourde, K., Gibert, D., Marteau, J., de Bremond d'Ars, J., Gardien, S., Girerd, C., Ianigro, J.-C. and Carbone, D.: Experimental detection of upward going cosmic particles and consequences for correction of density radiography of volcanoes, Geophys. Res. Lett., 40, 6334–6339, doi:10.1002/2013GL058357, 2013.

Jourde, K., Gibert, D. and Marteau, J.: Improvement of density models of geological structures by fusion of gravity data and cosmic muon radiographies, Geosci. Instrumentation, Methods Data Syst. Discuss., 5, 83–116, doi:10.5194/gid-5-83-2015, 2015.

Kelner, S. R.: Pair Production in Collisions between Muons and Atomic Electrons, Phys. At. Nucl., 61, 448–456, 1998.

Kelner, S. R., Kokoulin, R. P. and Petrukhin, A. A.: About Cross Section for High-Energy Muon Bremsstrahlung, Prepr. Moscow Eng. Phys. Inst., 1–32, 1995.

Kelner, S. R., Kokoulin, R. P. and Petrukhin, A. A.: Bremsstrahlung from Muons Scattered by Atomic Electrons, Phys. At. Nucl., 60, 576–583, 1997.

Kokoulin, R. P. and Petrukhin, A. A.: Analysis of the Cross-Section of Direct Pair Production by Fast Muons, in Proceedings of the 11th Conference on Cosmic Rays, pp. 277–284, Budapest., 1969.

Kokoulin, R. P. and Petrukhin, A. A.: Influence of the Nuclear Formfactor on the Cross-Section of Electron Pair Production by High Energy Muons, in Proceedings of the 12th International Conference on Cosmic Rays, p. 1446, Tasmania, Australia., 1971.

Lesparre, N., Gibert, D., Marteau, J., Déclais, Y., Carbone, D. and Galichet, E.: Geophysical muon imaging: feasibility and limits, Geophys. J. Int., 183, 1348–1361, doi:10.1111/j.1365-246X.2010.04790.x, 2010.

Lesparre, N., Gibert, D., Marteau, J., Komorowski, J.-C., Nicollin, F. and Coutant, O.: Density muon radiography of La Soufrière of Guadeloupe volcano: comparison with geological, electrical resistivity and gravity data, Geophys. J. Int., 190, 1008–1019, doi:10.1111/j.1365-246X.2012.05546.x, 2012.

Lohmann, W., Kopp, R. and Voss, R.: Energy Loss of Muons in the Range of 1-10000 GeV., 1985.

Mando, M. and Ronchi, L.: On the Energy Range Relation for fast Muons in Rock ., Nuovo Cim., 9, 517–529, 1952.

Marteau, J., Carlus, B., Gibert, D., Ianigro, J.-C., Jourde, K., Kergosien, B. and Rolland, P.: Muon tomography applied to active volcanoes, in International Conference on New Photo-detectors, PhotoDet2015, pp. 1–7, Moscow. [online] Available from: http://arxiv.org/abs/1510.05292, 2015.

Matter, A., Homewood, P., Caron, C., Rigassi, D., Stuijvenberg, J., Weidmann, M. and Winkler, W.: Flysch and molasse of western and central Switzerland, in Flysch and molasse of western and central Switzerland, pp. 261–292, Wepf., 1980.

Miyake, S., Narashimham, V. S. and Ramana Murthy, P. V.: Cosmic-Ray Intensity Measurements Deep Underground at Depths of (800-8400) m.w.e., Nuovo Cim., 32, 1505–1523, 1964.

Morishima, K., Kuno, M., Nishio, A., Kitagawa, N., Manabe, Y., Moto, M., Takasaki, F., Fujii, H., Satoh, K., Kodama, H., Hayashi, K., Odaka, S., Procureur, S., Attié, D., Bouteille, S., Calvet, D., Filosa, C., Magnier, P., Mandjavidze, I., Riallot, M., Marini, B., Gable, P., Date, Y., Sugiura, M., Elshayeb, Y., Elnady, T., Ezzy, M., Guerriero, E., Steiger, V., Serikoff, N., Mouret, J.-B., Charlès, B., Helal, H. and Tayoubi, M.: Discovery of a big void in Khufu's Pyramid by observation of cosmic-ray muons, Nature, 552, 386–390, doi:10.1038/nature24647, 2017.

Neddermeyer, S. H. and Anderson, C. D.: Note on the Nature of Cosmic-Ray Particles, Phys. Rev., 51, 884–886, 1937.

Nikishov, A. I.: Energy spectrum of e+e- pairs produced in the collision of a muon with an atom, Sov. J. Nucl. Phys., 27, 677–681, 1978.

Nishiyama, R., Tanaka, Y., Okubo, S., Oshima, H., Tanaka, H. K. M. and Maekawa, T.: Integrated processing of muon radiography and gravity anomaly data toward the realization of high-resolution 3-D density structural analysis of volcanoes: Case study of Showa-Shinzan lava dome, Usu, Japan, J. Geophys. Res. Solid Earth, 119, 699–710, doi:10.1002/2013JB010234, 2014.

Nishiyama, R., Ariga, A., Ariga, T., Käser, S., Lechmann, A., Mair, D., Scampoli, P., Vladymyrov, M., Ereditato, A. and Schlunegger, F.: First measurement of ice-bedrock interface of alpine glaciers by cosmic muon radiography, Geophys. Res. Lett., doi:10.1002/2017GL073599, 2017.

Olive, K. A. et al. (Particle Data Group): Review of Particle Physics, Chinese Phys. C, 38, 090001, doi:10.1088/1674-1137/38/9/090001, 2014.

Reyna, D.: A Simple Parameterization of the Cosmic-Ray Muon Momentum Spectra at the Surface as a Function of Zenith Angle, [online] Available from: http://arxiv.org/abs/hep-ph/0604145, 2006.

Richard-Serre, C.: Evaluation de la perte d'energie unitaire et du parcours pour des muons de 2 à 600 GeV dans un absorbant quelconque., 1971.

Seltzer, S. M. and Berger, M. J.: Evaluation of the Collision Stopping Power of Elements and Compounds for Electrons and Positrons, Int. J. Appl. Radiat. Isot., 33, 1189–1218, 1982.

Sternheimer, R. M., Seltzer, S. M. and Berger, M. J.: Density effect for the ionization loss of charged particles in various substances, Phys. Rev. B, 26, 6067–6076, 1982.

Sternheimer, R. M., Berger, M. J. and Seltzer, S. M.: Density Effect for the Ionization Loss in Various Substances, At. Data Nucl. Data Tables, 30, 261–271, 1984.

Stoer, J. and Bulirsch, R.: Introduction to Numerical Analysis, Springer New York, New York, NY., 2002.

Strunz, H. and Nickel, E.: Strunz Mineralogical Tables. Ninth Edition, Schweizerbart Science Publishers, Stuttgart, Germany., 2001.

Tanaka, H. K. M., Nagamine, K., Nakamura, S. N. and Ishida, K.: Radiographic measurements of the internal structure of Mt. West Iwate with near-horizontal cosmic-ray muons and future developments, Nucl. Instruments Methods Phys. Res. Sect. A Accel. Spectrometers, Detect. Assoc. Equip., 555, 164–172, doi:10.1016/j.nima.2005.08.099, 2005.

Tanaka, H. K. M., Kusagaya, T. and Shinohara, H.: Radiographic visualization of magma dynamics in an erupting volcano, Nat. Commun., 5, 1–9, doi:10.1038/ncomms4381, 2014.

Tuttle, O. F. and Bowen, N. L.: Origin of granite in the light of experimental studies in the system NaAlSi3O8-KAlSi3O8-SiO2-H2O, Geol. Soc. Am. Mem., 74, 1–146, 1958.

Solid Earth Discuss., https://doi.org/10.5194/se-2018-46
Manuscript under review for journal Solid Earth
Discussion started: 8 June 2018

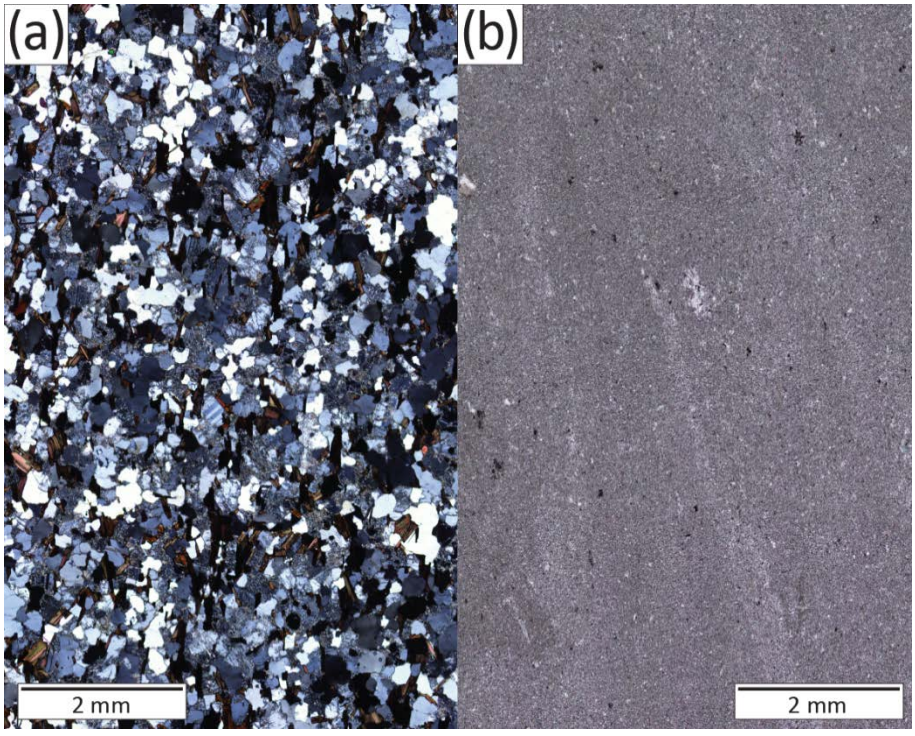

480 **Figure 1: Thin-sections of two representative types of rock in crossed polarised light: (a) Granite, (b) Limestone. The crystal sizes are generally below 1 mm and a few orders of magnitude smaller in the limestone.**

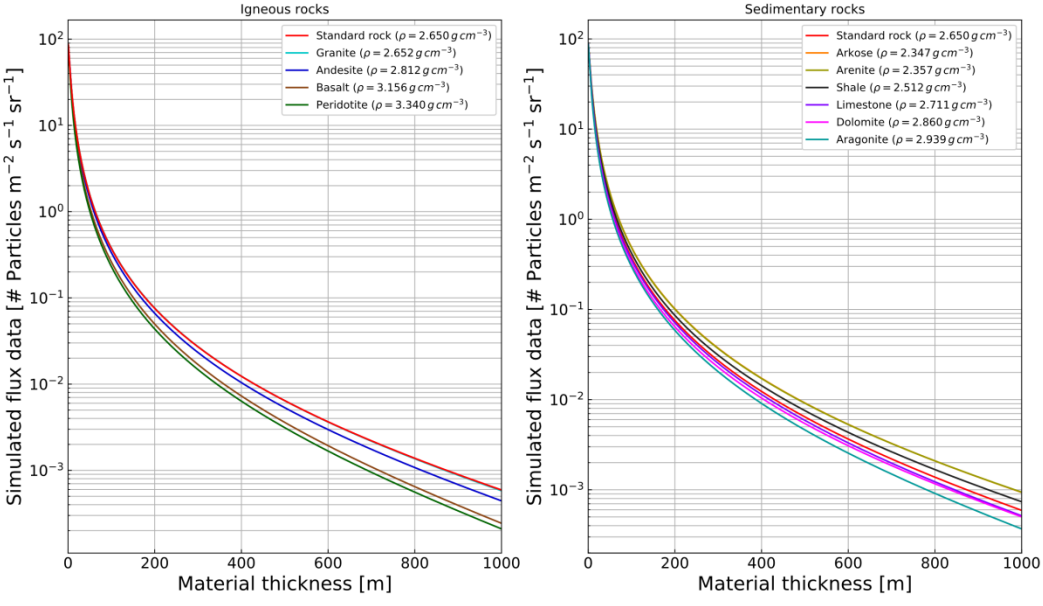

Figure 2: Simulated muon intensity vs thickness of the four igneous, six sedimentary rocks from Table 1 and standard rock.

Solid Earth Discuss., https://doi.org/10.5194/se-2018-46
Manuscript under review for journal Solid Earth
Discussion started: 8 June 2018

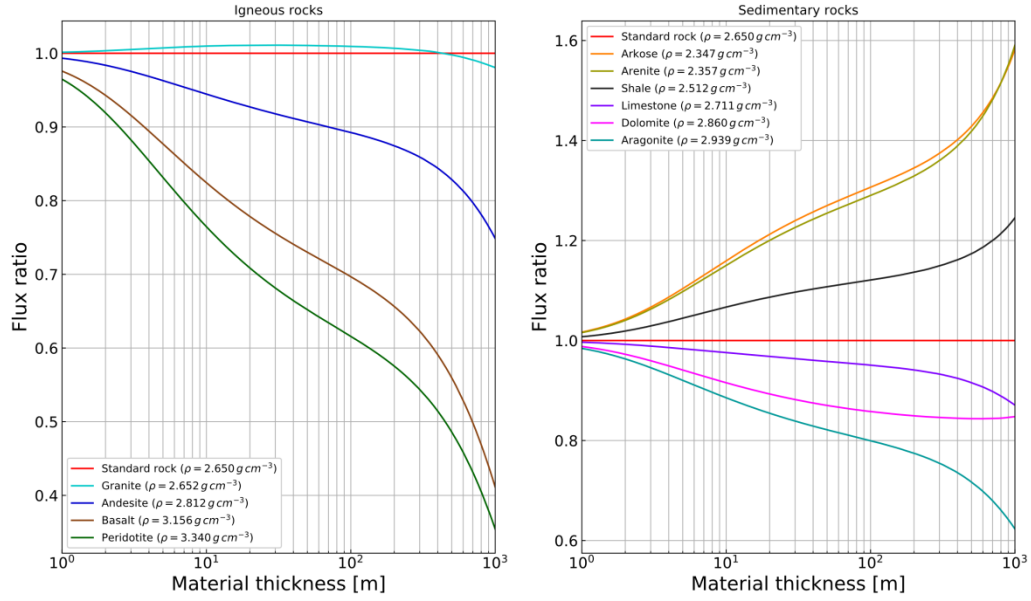

485 **Figure 3: Ratio of the calculated rock fluxes to a standard rock muon flux for all the rocks reported in Table 1 as a function of rock thickness.**

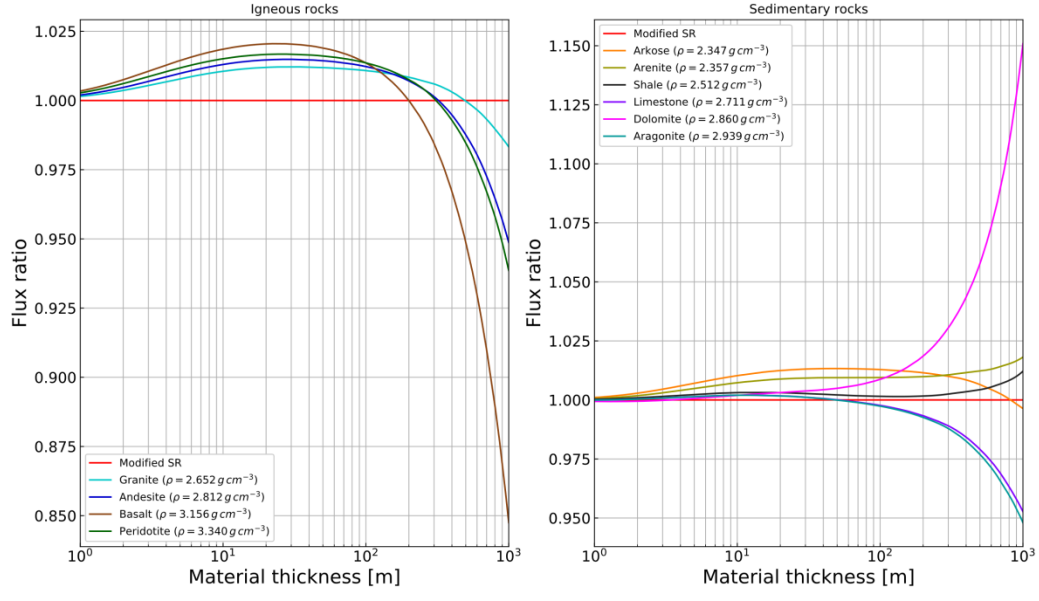

Figure 4: Ratio of the calculated rock fluxes to a standard rock muon flux with the same density as the rock ($\rho_{SR} = \rho_{Rock}$) for all the lithologies reported in Table 1 as a function of rock thickness.

490

Solid Earth Discuss., https://doi.org/10.5194/se-2018-46
Manuscript under review for journal Solid Earth
Discussion started: 8 June 2018

Table 1: Physical parameters of the ten studied rock types and of standard rock.

Rock	Density $[g/cm^{-3}]$	{Z/A}	$\{Z^2/A\}$	$\{Z^2/A\}/\{Z/A\}$	{I} $[eV]$
Standard rock	2.650	0.5000	5.500	11.0	136.40
Igneous rocks					
Granite/Rhyolite	2.652	0.4966	5.650	11.38	145.27
Andesite/Diorite	2.812	0.4960	5.803	11.70	147.77
Gabbro/Basalt	3.156	0.4945	6.238	12.62	154.91
Peridotite	3.340	0.4955	5.790	11.69	149.98
Sedimentary rocks					
Arkose	2.347	0.4980	5.563	11.17	143.73
Arenite (Sandstone)	2.357	0.4993	5.392	10.80	141.04
Shale	2.512	0.4994	5.385	10.78	139.09
Limestone	2.711	0.4996	6.275	12.56	136.40
Dolomite	2.860	0.4989	5.423	10.87	127.65
Aragonite	2.939	0.4996	6.275	12.56	136.40

Table A1: Volumetric percentages of the rock forming minerals within six sedimentary rocks. Qtz: Quartz, Or: Orthoclase, Ab: Albite, An: Anorthite, Cal: Calcite, Dol: Dolomite, Kln: Kaolonite, Mnt: Montmorillonite, Ill: Illite, Clc: Clinochlore

Mineral	Arkose	Arenite	Shale	Limestone	Dolomite	Aragonite
Qtz	56.0	89.0	17.0			
Or	34.0		2.5			
Ab			1.8			
An			0.7			
Cal				100.0		100.0
Dol					100.0	
Kln			1.7			
Mnt			52.7			
Ill			22.2			
Clc			1.4			
Air	10.0	11.0				

Solid Earth Discuss., https://doi.org/10.5194/se-2018-46
Manuscript under review for journal Solid Earth
Discussion started: 8 June 2018

Table A2: Volumetric percentages of the rock forming minerals within four igneous rocks. Qtz: Quartz, Or: Orthoclase, Ab: Albite, An: Anorthite, Phl: Phlogopite, Ann: Annite, Mg-Hbl: Magnesium hornblende, Fe-Hbl: Iron hornblende, Aug: Augite, En: Enstatite, Fs: Ferrosilite, Fo: Forsterite, Fa: Fayalite, Jd: Jadeite, Hd: Hedenbergite, Di: Diopside, Spl: Spinel, Hc: Hercynite

Mineral	Granite	Andesite	Basalt	Peridotite
Qtz	36.1	11.7		
Or	28.2			
Ab	27.3	37.7	17.7	
An		25.3	24.6	
Phl	2.95	4.5		
Ann	2.95	2.1		
Mg-Hbl	2.25	4.2		
Fe-Hbl	2.25	6.4		
Aug		8.1	33.8	
En			11.4	18.4
Fs			11.1	2.0
Fo			0.6	60.4
Fa			0.8	7.9
Jd				1.8
Hd				0.3
Di				8.0
Spl				0.9
Hc				0.3